Thermal interactions between nucleation sites and the solid wall during pool boiling of a pure fluid: A review

A. Marie, S. Cioulachtjian, S. Lips, V. Sartre

▶ **To cite this version:**

A. Marie, S. Cioulachtjian, S. Lips, V. Sartre. Thermal interactions between nucleation sites and the solid wall during pool boiling of a pure fluid: A review. International Journal of Thermal Sciences, 2022, 174, pp.107388. 10.1016/j.ijthermalsci.2021.107388 . hal-04074470

HAL Id: hal-04074470
https://hal.science/hal-04074470v1

Submitted on 22 Jul 2024

HAL is a multi-disciplinary open access archive for the deposit and dissemination of scientific research documents, whether they are published or not. The documents may come from teaching and research institutions in France or abroad, or from public or private research centers.

L'archive ouverte pluridisciplinaire **HAL**, est destinée au dépôt et à la diffusion de documents scientifiques de niveau recherche, publiés ou non, émanant des établissements d'enseignement et de recherche français ou étrangers, des laboratoires publics ou privés.

Distributed under a Creative Commons Attribution - NonCommercial 4.0 International License

Version of Record: https://www.sciencedirect.com/science/article/pii/S1290072921005433
Manuscript_098d94a373df1bf24e854100caa1add8

Thermal interactions between nucleation sites and the solid wall during pool boiling of a pure fluid: a review

A. Marie[a], S. Cioulachtjian[a], S. Lips[a], V. Sartre[a]

[a] *Univ Lyon, INSA Lyon, CNRS, CETHIL, UMR5008, 69621 Villeurbanne, France*

Abstract

This paper reviews the various effects of the coupling between thermal conduction within a heated wall and the growth of vapor bubbles in saturated pure liquids. In a first part, numerical and experimental investigations of single-site nucleation coupled with solid conduction within the wall are reviewed. The numerical investigations demonstrate that the wall temperature drop induced by bubble nucleation is significantly increased when the wall thermal diffusivity is decreased. Furthermore, bubble generation appears to be greatly inhibited by a reduction of the wall diffusivity. Concurrently, newly developed experimental methods provide promising insights on solid/fluid coupling in single site nucleation. In particular, several studies highlights the link between a sustained temperature drop beneath a growing bubble and the vaporisation of a liquid micro-layer deposited during bubble growth. Finally, conclusions raised by the existing literature in various configurations of multi-site boiling are detailed and compared. On one hand, the radius of thermal influence of a bubble inferred by these studies are comparable (between 1.5 and 3 times the bubble diameter). On the other hand, it is still difficult to provide a general criterion predicting this interaction range as a function of the wall thermal properties.

Keywords: Pool boiling, Conduction, Bubble growth, Nucleation sites interaction, Wall characteristics

Contents

1. Introduction

The numerical and experimental studies of pool boiling have been a very active field of research for many decades [1–3]. Indeed, it is a very complex phenomenon involving, among others, heat and mass transfer within a liquid/vapor flow, dynamic wettability effects as well as thermal interactions with the heated wall. At the same time, as nucleate boiling is a very efficient way to dissipate heat, practical applications of pool boiling are numerous. For instance, boiling of a working fluid inside the evaporator of a thermosyphon is often considered for the thermal management of electronic components [4–6].

A common need for this type of application is the availability of reliable heat transfer predictive tools. Indeed, the knowledge of boiling heat transfer coefficient as well as critical heat flux is necessary to design such cooling systems. At the moment, empirical correlations are often used to predict boiling heat transfer. However, as highlighted by Mohanty & Das[7], if these correlations are relatively efficient in predicting the experimental results of their authors, they are much less reliable when compared with data of other investigators. In particular, one of the conclusions of this review was that most correlations relied on bubble dynamic parameters (nucleation frequency, bubble departure diameter and nucleation site density in particular) which were also evaluated with empirical correlations. This was pointed out by the authors as the reason why most pool boiling heat transfer correlations failed

© 2021 published by Elsevier. This manuscript is made available under the CC BY NC user license
https://creativecommons.org/licenses/by-nc/4.0/

at predicting different experiments. Hence, it seems that more fundamental understanding of the numerous physical factors influencing boiling dynamics is necessary.
To this aim, more specific theoretical works have been performed in the past decades, with the objective of providing understanding of the different fundamental phenomena linked to vapor nucleation on a heated surface. For example, the influence of the fluid wettability on pool boiling has been recently reviewed by Malavasi et al. [8]. Similarly, the distribution of the dissipated heat flux between liquid micro-layer evaporation, bubble liquid/vapor interface and transient conduction from the superheated wall to colder liquid has been the subject of a comprehensive review by Kim [9]. The effect of the wall geometry at nano, micro and macro scales on boiling heat transfer coefficient and critical heat flux has been thoroughly reviewed by Liang et al. [10]. Finally, the effect of the application of electric fields on boiling heat transfer has been reviewed by Shahriary et al. [11].
However, the interaction betwen heat transfer in the solid wall and the two-phase flow associated to bubble growth and departure seems to be a much less discussed topic. Indeed, to the best of the authors' knowledge, the coupling of nucleate boiling and conduction within the heated wall was only briefly addressed in more general reviews [12, 13]. Considering this, the present review paper aims at providing an outlook of the available knowledge concerning the impact of conduction within the solid wall on the heat and mass transfer in situation of pool boiling. To this aim, numerical and experimental investigations of single site nucleate boiling are reviewed in a first part. Then, published articles involving multiple nucleation sites are presented. The active enhancement methods (electric or magnetic fields, ultrasounds...) are not considered here.
This analysis of the existing studies may enable to highlight the key parameters affecting the fluid/wall interaction during pool boiling and the remaining scientific questions that need to be answered before being able to develop effective predictive tools.

2. Interaction between a single nucleation site and the wall

In this section, the studies addressing the coupling between bubble growth and heat diffusion within the wall in the simplest case of bubble generation on a unique nucleation site are presented. In a first part, the existing numerical approaches are presented. Then, publications which provide insights of the wall/fluid coupling with the help of experimental methods are detailed.

2.1. Numerical investigations

Numerical modelling allows to evaluate the temperature distribution within the heated wall and to easily investigate the influence of the wall thermal properties. To this aim, many numerical approaches have been proposed to evaluate the transient wall response influence on a single bubble nucleation cycle [14–31]. In a first part, the various formulations of these models are presented. Thereafter, the corresponding thermal response and bubble dynamics are displayed.

2.1.1. Formulation of the models

In a general manner, as it is represented on Fig.1, the nucleation cycle can be separated into two phases : a bubble growth time t_g and a waiting time t_w. Considering this, one of the simplest configurations seems to be the one proposed by Wang et al [30]. In their publication, they proposed several analytical solutions of transient conduction within the heated wall during the aforementioned waiting time t_w. To allow for simple solutions of this problem, the wall temperature was supposed to vary only within its thickness and heat transfer at the solid/liquid boundary was based on the calculation of a developing thermal boundary layer in the liquid.

Apart from this very specific case, multidimensional heat conduction is considered in the solid region and phase change is modeled within the fluid domain. As represented on the central part of Fig. 2, the computational problem is then generally considered to be axisymmetric around a vertical axis going through the nucleation site. Additionally, a three-dimensional configuration in which heat diffusion and fluid flows are solved within a cubic numerical domain has been adressed in a few recent publications [28, 31]. One advantage of this type of models is that contrary to axisymmetric models, the computation of multiple nucleation sites may be possible in the future. However, in the single site configurations they considered, only a quarter of the bubble surroundings has been be computed thanks to symmetry considerations.

Concerning heat conduction within the wall, classical numerical procedures such as finite difference schemes are usually applied to solve the heat equation, generally written in axisymmetric form. To address the more complex numerical issue of phase change within the fluid, different types of approaches are implemented. Early models [14–16] considered a simplified case in which the thermal and hydraulic phenomena modelisation was limited to the evaporation of a thin liquid layer at the base of the bubble, i.e. heat and fluid flows around the bubble were not solved. More recently, a similar resolution based on simplifications of the heat and fluid flows in the liquid phase was also implemented by Jiang et al. with a view to a future integration as a single nucleation site submodel in a complete CFD resolution which could involve multiple bubbles and external fluid flow [22]. Otherwise, most of the models published in the last two decades are based on a complete resolution of the heat and mass transfer associated to bubble growth and departure [17–21, 23, 24, 27–29, 31]. In most cases, the bubble nucleation

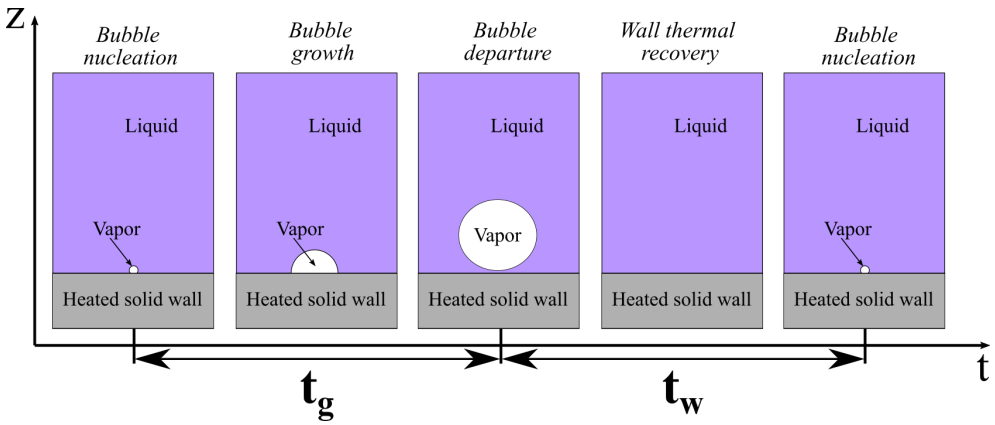

Figure 1: Schematic characterization of the different phases of a bubble nucleation period and associated characteristic times

is initiated at a given threshold superheat of the nucleation site by the adjunction of a small bubble serving as a vapor seed [20, 23, 24, 27–29, 31]. Then various numerical techniques are used to dynamically evaluate the bubble interface shape, the vaporization flow rate at the interface, the heat transfer rates in the micro-region layers or in the elongated films and the contact line movement. The detail of these numerical procedures is beyond the scope of the current review and will therefore not be discussed in more depth here. For precise descriptions of these techniques, the reader should refer to dedicated reviews, see for example the summary proposed by Kharangate & Mudawar [32].

However, an important distinction between two types of model can be made here. Indeed, two different shapes of the liquid vapor interface at the junction between the liquid/vapor interface and the wall are assumed depending on the authors cited therafter. A first group of publications [17–21, 23, 24, 26, 27] only considers the existence of a micro-region at the triple line region of the bubble. In other words, the calculation of the interface shape in this area is derived from the triple line evaporation model proposed by Stephan & Busse [33]. This model is based on the mass and momentum conservation equations, the augmented Laplace-Young equation, and the Fourier law, including an interfacial resistance and assuming liquid-vapor equilibrium. In this case, as represented on the right part of Fig. 2, the interface at the base of the bubble is divided in three parts : the bulk meniscus, a short micro-region typically less than one micrometer long within which very intense heat transfer takes place and a non-evaporating adsorbed film.

Instead of a small micro-region area, a second group of publications assumes the existence of a thin elongated liquid film at the bubble base which is commonly referred as the micro-layer [14–16, 22, 28, 29, 31]. The liquid layer computed by these authors has a length typically ranging from a few hundreds of microns to a few millimeters. In this case, represented on the left part of Fig.2, it is assumed that the rapid recession of the liquid/vapor interface on the wall during bubble growth induces the retention of a thin liquid film along the bubble radius which then progressively evaporates during bubble growth. Various computational methods are proposed to take into account the micro-layer evaporation during bubble growth. One of the simplest implementations, proposed by Guo & El-Genk [14], only calculates the heat flow associated to the evaporation of the micro-layer. However, more recent studies (see for example the one of Giustini et al. [28]) incorporate a dedicated micro-layer sub-model in a CFD resolution of the two-phase flow associated to the bubble growth. In most cases, the liquid in the micro-layer is assumed to be stationary [14–16, 28, 29, 31], meaning that the variation of the liquid microlayer thickness with time is only computed as the consequence of static evaporation. Experimental or theoretical correlations are generally used to calculate the initial shape of the film. A more complete description of this complex phenomenon, beyond the scope of this review, can be found for instance in the coupled theoretical and experimental investigation of Jung et al. [34]. Finally, on this particular topic of interface geometry at the base of the bubble, it has to be noted that recent experimental investigations allowed to evaluate some parameters influencing the transition from micro-region to micro-layer deposition [35, 36]. In particular, micro-layer deposition was only observed when the receding interface velocity was high enough, while lower velocities only induced a micro-region at the contact line. In the case of bubble nucleation, this would mean that the biggest and fastest growing bubbles would induce micro-layers at their base while the smallest and slowest growing bubbles would not. However, there is not yet a validated criterion to distinguish between the two interface geometries, making it difficult to choose the adequate one in a numerical simulation.

2.1.2. Thermal response of the wall

In the simplest one-dimensional case considered by Wang et al. [30], the computation of analytical solutions asso-

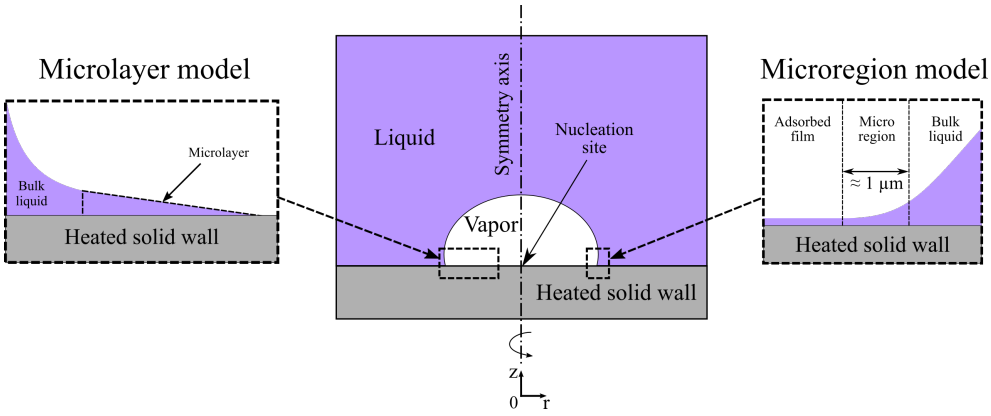

Figure 2: Axisymmetric configuration considered in the majority of bubble growth models presented in this review, adapted from Chen et al. [29] and Mann et al. [17]

ciated to the assumption of infinitely thin and infinitely thick heaters was developed. The comparison of these solutions to available experimental data corresponding to various heater materials demonstrated the influence of the assumed heater thickness on its temperature variation after bubble departure. These two analytical solutions also provided satisfying lower and upper bounds for the experimental temperature variation under certain conditions (moderate heat fluxes and waiting time significantly longer than the bubble growth duration). However, the specific effect of the wall material was not thoroughly discussed.
On the contrary, in the model of Mann et al. [17], in which heat and fluid flows are solved with the assumption of a short micro-region at the base of the bubble, the thermal response of the wall is compared for three different materials : ceramic, stainless steel and copper. As represented on Fig. 3 in which the wall temperature distribution beneath a bubble of a given size is represented for three different materials, the copper wall appears to stay almost isothermal during bubble growth. On the contrary, the ceramic wall exhibits a very particular temperature drop, especially pronounced at the area in contact with the computed micro-region. In addition, they showed that the ceramic wall induced a 40% lower heat flux passing through the micro-region due to poor thermal conduction preventing heat flow redistribution within the wall. The wall effect on the heat flux dissipation associated to bubble nucleation was later evaluated in more details [18, 19]. In these studies, based on similar models, authors stated that despite very small spatial temperature gradients within the wall in the specific case of a highly conductive copper wall, the variation of sensible heat stored in the wall could not be neglected in front of the heat absorbed by the growing bubble. In the specific case of a heated stainless steel foil, Kunkelmann et al. [20] showed that the heat flux evacuated by the micro-region area was higher during the departing bubble phase (advancing contact line) than during its growth (receding contact line). This was explained by the thermal history of the wall. Indeed, during departure, the micro-region comes in contact with a formerly dried out wall having a higher local superheat than in the bubble base expansion phase (where the triple line recedes into an area initially covered with liquid).

The model developed by Aktinol and Dhir [21], con-

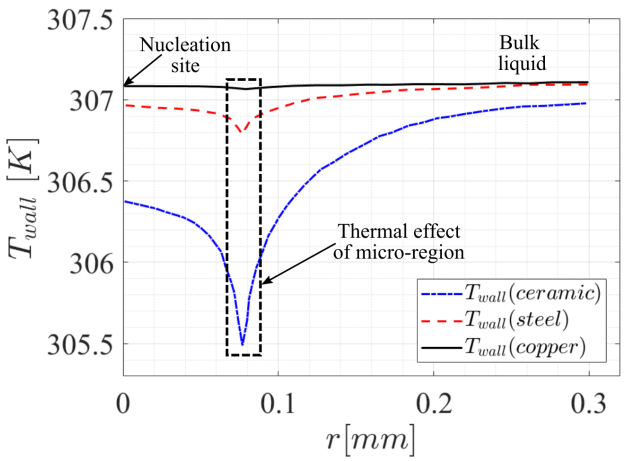

Figure 3: Computed variation of the wall temperature distribution at a time step corresponding to the same bubble size for three different materials, adapted from Mann et al. [17]

sidering the same geometry of micro-region at the junction between the liquid/vapor interface and the solid wall, corroborates the influence of the wall thermal properties on both the associated numerical temperature drops and peaks in heat flux induced by bubble development. In particular, for a borosilicate glass heated wall, local temperature drops representing more than 90% of the initial superheat were highlighted by the model. Concurrently, while heat flux peaks in the micro-region area as high as 136 times the input heat flux were highlighted in the case of a copper wall, this ratio was lowered to less than 80 in the case of borosilicate glass. In the numerical studies conducted by Zhang et al. [23] as well as Li et al. [24], the

micro-region geometry was simplified by assuming a constant slope of the liquid/vapor interface in this area. This simplification did however not change the general response of the simulated heater. In particular, temporal and spatial thermal gradients in the vicinity of the contact line were shown to increase when the wall thermal diffusivity was decreased. A different conclusion was drawn in the numerical investigation developed by Huber et al. [27]. It was indeed shown that the heat diffusion within the wall had a very limited effect during the entire bubble growth. To be noted that, according to the authors of this study, this conclusion was appropriate because of the high thermal diffusivity of the 1.3 mm thick silicon substrate considered in their study. Hence, different observations might be made for thinner and less conductive heaters.

Otherwise, when a micro-layer is implemented on the solid wall located within the bubble, the temperature response predicted by the published models exhibits a shape significantly different from the one obtained when only the micro-region is considered. Indeed, instead of a sharp temperature drop at the micro-region position, transient cooling of the wall associated to the bubble growth is predicted along a much longer radius roughly corresponding to the micro-layer length (generally comprised between 0.1 and 1 mm while a micro-region length is of the order of one micrometer). This characteristic shape of the radial wall temperature during bubble growth is for instance highlighted by Chen et al. [29] in the case of a poorly conductive glass wall, as represented on Fig. 4. In this publication, they show that poorly conductive materials tend to reduce the heat flow that can be brought to the micro-layer from the heated wall, which prolongs its presence at the base of the bubble and the corresponding cooling of the wall. To

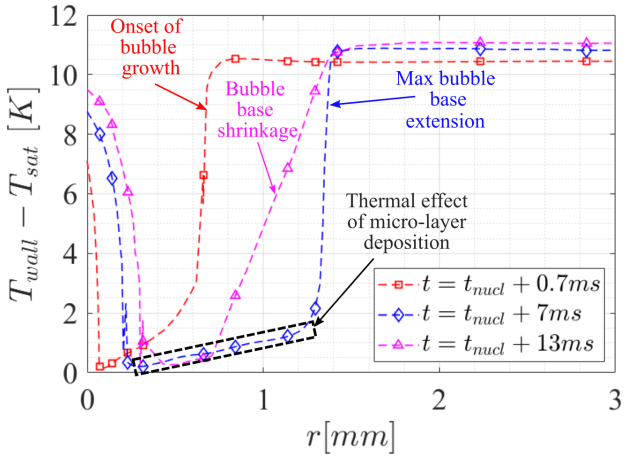

Figure 4: Temperature profile beneath the bubble on a glass wall at different time step after nucleation at $t = t_{nucl}$, adapted from Chen et al. [29]

be noted that these observations are qualitatively consistent with the conclusions of similar previous studies based on simpler models [14, 16]. Comparable temperature distributions beneath the bubble were highlighted by Jiang et al. [22]. In addition, in the particular case of a 2 mm thick stainless steel heater, the existence of a low superheat area beneath the micro-layer has also been demonstrated by Giustini et al. [28].

2.1.3. Impact on nucleation dynamics

In the same way that the computed thermal response of the wall was shown to be highly dependant on the wall thermal properties, some of the aforementionned publications demonstrated a strong material influence on the nucleation dynamics, i.e. the bubble diameter at departure D_b, the bubble growth time t_g (the time interval between the growth start of the bubble and its departure) and waiting time t_w(duration between bubble release and the following bubble growth start). Once again, the impact of various wall materials on the nucleation dynamics appears to be dependant of the interface geometry at the junction of the bubble interface and the wall.

On one hand, in the case where only a micro-region is considered beneath the bubble, it is shown in the numerical study of Aktinol et al. [21] that, under the same heat flux, the waiting time t_w is multiplied by around five for borosilicate glass compared to a plain copper wall. On the contrary, the bubble growth rate and departure diameter D_d itself are very slightly increased when the wall material diffusivity is decreased. This behavior is explained by the fact that more thermally resistive surfaces tend to induce thicker thermal boundary layer as a consequence of longer waiting times. Hence, the overall warmer liquid increases the heat flux absorbed by the bubble from its surrounding liquid, resulting in slightly larger bubbles. The same trend is exhibited by Zhang et al. [23]. In particular, for the same wall thickness, a thermally insulative fused silica wall is shown to induce a waiting time more than 500 times higher than in the case of the highly conductive nickel wall. It has however to be noted that, since only the bottom wall superheat is imposed in this study, the heat flux supplied to the fluid is not held constant when the material is changed. Finally, this effect of transient conduction in the wall has also been witnessed by Huber et al. [27], as taking into account conduction within the wall slightly increases the bubble growth compared to the isothermal case. The observed impact is however very small as the silicon wall considered in this case has a very high thermal conductivity.

On the other hand, conclusions raised by the authors considering a micro-layer beneath the bubble seems to differ significantly from the results exposed above. Firstly, Guo & El-Genk [14] obtained a significantly faster bubble growth for pure copper substrates compared to the one covered with an insulating glass layer. This behavior is explained by the fact that poorly conductive walls are associated with significant local cooling of the solid beneath the liquid vapor interface, reducing the local heat flux pass-

ing through the liquid micro-layer, hence moderating its vaporization. The more recent study of Giustini et al. [28] agrees with this observation, as the bubble growth rate is showed to be lower for a stainless steel wall than for a copper wall of similar geometry. Finally, in the numerical study of Chen et al. [29], the computed bubble volume at departure is about fourteen times lower with a glass heater than in the case of a copper wall, as represented on Fig. 5 for a constant heat input and nucleation superheat. Additionally, as concentration of the conductive heat flux towards the micro-layer was limited when the wall diffusivity was decreased, they show that a more significant part of the vaporisation heat flux is redirected through the bulk liquid into the spherical interface of the bubble.

However, the impact of the wall material on the waiting

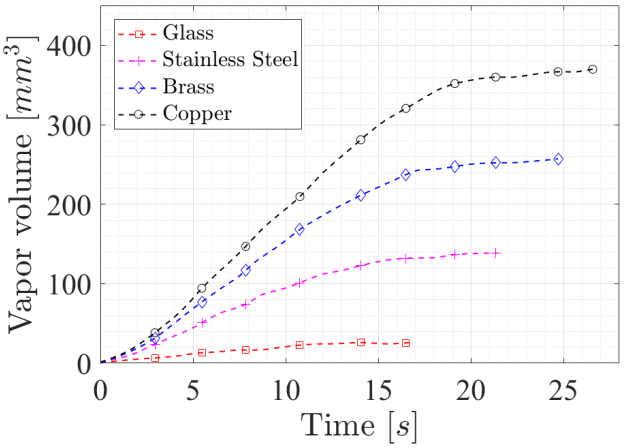

Figure 5: Influence of wall material on the vapor volume growth, reproduced from Chen et al. [29]

time in the case where a micro-layer is considered beneath the bubble has not been discussed by the aforementionned authors. Indeed, Guo & El-Genk [14] considered it as a parameter of the numerical model and the other studies mentioned in this paragraph were limited to the bubble growth period.

The qualitative influence of the wall thermal diffusivity α_s on the bubble dynamics is synthetized in table 1 in which $D_b(\alpha_s)$, $t_g(\alpha_s)$ and $t_w(\alpha_s)$ represent the evolution with the wall thermal diffusivity of the bubble diameter at departure, bubble growth time and waiting time respectively. The boundary condition imposed on the solid wall to induce heat dissipation is detailed in the corresponding column and the parameter δ_{wall} represents the thickness of the wall considered within the models. Given that all the studies listed in this table consider the same working fluid as well as comparable wall thickness and thermal diffusivity range, a few interesting tendancies can be highlighted again to conclude this section. Concerning bubble growth time, the different models agree on the general tendancy, i.e. a positive variation of the growth time t_g with the wall thermal diffusivity is predicted in all cases. It is to be noted however that the variation of t_g seems to be largely more important in the micro-layer models. Additionally, two publications agree on the fact that the waiting time t_w is strongly decreased when the wall thermal diffusivity α_s is increased.

On the other hand, there is a remarkable contradiction on the bubble diameter at departure D_b as models considering a micro-region predicts a decrease in D_b when the wall thermal diffusivity is increased while models including a micro-film indicate the exact opposite.

To conclude this part of the review, the findings on which the published numerical studies can be considered globally concurring can be succintly summarized. Indeed, the aforementionned paper globally concludes that low diffusivity walls are more subjected to temperature drops during bubble nucleation. Furthermore, the wall thermal response tends to mitigate the volume of vapor produced per unit of time at a given nucleation site, particularly in the case of micro-layer deposition.

2.2. Experimental studies of the wall thermal response

Concurrently to the numerical investigations presented above, various experimental approaches have been developed to evaluate the actual thermal response of a solid wall subjected to bubble nucleation and to correlate it with its observed geometrical evolution of the growing bubble. In a general manner, these publications aimed to provide new experimental insights of heat transfer within the wall associated with bubble formation on a single nucleation site. Additionally, this type of data can be later used to provide reference case to numerical models of single site pool boiling.

In a first part, the different experimental methods used to capture the solid wall temperature dynamic are presented. Thereafter, the results obtained by these experimental apparatus are outlined.

2.2.1. Experimental methods

Because of the very small time intervals and the sharp wall thermal gradients associated to the nucleation of a single bubble, accurate experimental characterization of the heater thermal response is considered as a very challenging task, as explained by Myers et al. [37]. To address this difficulty, they used an array of 96 micro-heaters laid on the wall to provide a uniform heat flux on a 500 µm thick silica substrate. These heaters were simultaneously used as thermistors to measure the local wall temperature beneath a growing bubble at a frequency of 1130 s^{-1}. A 3D numerical model of the heated wall was developed to deduce the spatial and temporal heat flux distributions from the upper wall temperature. Similarly, Moghaddam et al. embedded several temperature sensors on a thin silicon substrate covered by a poorly conductive ($\lambda_s \approx 0.3\ W.m^{-1}.K^{-1}$) 10 μm thick benzocyclobutene layer [38]. An homogeneous heat

Authors	Bubble base	α_s $[m^2/s]$	Boundary condition	δ_{wall}	Fluid	$D_b(\alpha_s)$	$t_g(\alpha_s)$	$t_w(\alpha_s)$
Aktinol et al. [21]	µ-region	10^{-6} to 10^{-4}	Constant heat flux	$0.2 - 2.5\ mm$	water	$\searrow$ ($\approx -10\%$)	$\nearrow$ ($\approx +10\%$)	$\searrow$ ($\approx -80\%$)
Zhang et al. [23]	µ-region	$7.7.10^{-7}$ to $1.9.10^{-5}$	Constant superheat	$0.5 - 1.5\ mm$	water	$\searrow$ ($\approx -10\%$)	$\nearrow$ ($\approx +5\%$)	$\searrow$ ($\approx -99.9\%$)
Huber et al. [27]	µ-region	9.10^{-5} to ∞	Constant superheat	$1.2\ mm$	water	$\searrow$ ($\approx -1\%$)	$\nearrow$ ($\approx +1\%$)	-
Guo & El-Genk [14]	µ-layer	$6.9.10^{-7}$ to $1.1.10^{-4}$	Volumetric heat generation	$0.5 - 3.2\ mm$	water	$\nearrow$	-	-
Chen et al. [29]	µ-layer	$5.5.10^{-7}$ to $1.1.10^{-4}$	Constant heat flux	$2\ mm$	water	$\nearrow$ ($\approx +60\%$)	$\nearrow$ ($\approx +60\%$)	-
Giustini et al. [28]	µ-layer	$4.1.10^{-6}$ to $1.1.10^{-4}$	Constant heat flux	$2\ mm$	water	$\nearrow$ ($\approx +25\%$)	$\nearrow$ ($\approx +25\%$)	-

Table 1: Range of solid thermal diffusivities considered by published models and qualitative effects on the bubble dynamics

flux is applied by a thin film heater deposited on the back side to induce phase change of FC-72. A comparable setup based on sensors integrated within the substrate has also been used by Yabuki et al. [39] to study nucleate boiling of water on a 186 μm thick silicon substrate.

Concurrently, significant progress in high speed IR measurements techniques allowed to simplify the investigation of spatial and temporal temperature variations of the wall. Indeed, contrary to embedded micro-sensors, the use of IR camera filming the heater from the outside allows a very fine and non-intrusive spatial determination of the heated wall temperature. Using this technique, Golobic et al. demonstrated the possibility of simultaneous high speed bubble growth visualisations and IR temperature measurement of the heater backside [40]. In this case, an electrically heated 6 μm thin platinium foil was used as the heating surface and a transient conduction numerical model was used to deduce the local heat fluxes and heat transfer coefficients from the wall temperature variation. A similar experimental setup was also developed by Wagner & Stephan [41]. In their experiments, an electrically heated 20 μm thin stainless steel foil was used to generate boiling of the dielectric fluids FC-84 & FC-3284. Simultaneous visible and IR visualisations were performed and a 2D numerical model was used to obtain local heat fluxes. A comparable setup was developed by Gerardi et al. [42] to investigate pool boiling of deionized water on a 400 μm thick sapphire substrate heated with a thin ITO film deposited on the surface in contact with water. This apparatus was later improved by Duan et al. [43] through the addition of particle image velocimetry to investigate the liquid flow velocity fields around the bubble. More recently, two hydrophobic ITO-coated glass and sapphire substrates were investigated with IR and visible high speed cameras by Kangude & Srivastava [44].

Finally, as it is schematically represented on Fig.6, Jung & Kim combined IR and visible visualisations to optical interferometry in their pool boiling test bench [45]. Contrary to the aforementionned studies where the bubble geometry close to the wall could only be qualitatively inferred from the temperature field, this setup allows to directly identify the existence of a micro-layer beneath the bubble and to determine its geometry. In this case, a pool of deionized water is boiled on a transparent calcium fluoride substrate and a transient 3-dimensional model of the heated wall is developed to deduce the local heat flux exchanged with the fluid from the measured temperature fields. Thus, the local heat transfer coefficients beneath the bubble can be computed.

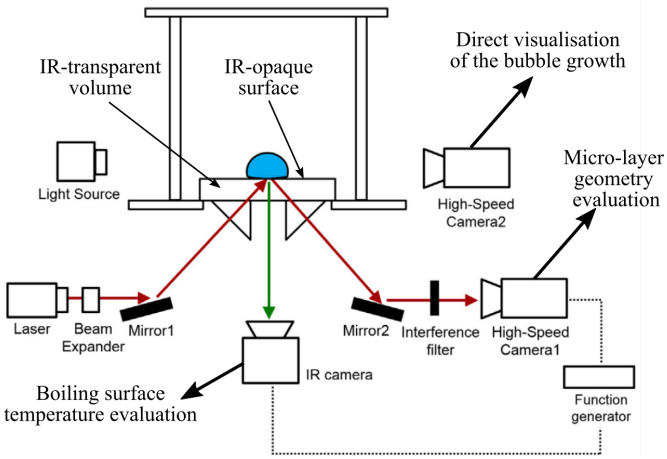

Figure 6: Experimental setup used in the study of Jung & Kim, reproduced from Jung & Kim [45]

2.2.2. *Results and analysis of the bubble/wall thermal coupling*

Thanks to their embedded temperature sensors, Myers et al. [37] could evaluate that the highest heat transfer intensity was measured during the liquid rewetting associated to the bubble departure. However, spatially averaged heater temperatures were predominantly detailed. Hence, the local temperature response of the wall was only briefly discussed.

On the contrary, spatial variations of the wall temperature have been investigated in more details by Moghaddam et al. [38]. Indeed, since a sustained cooling effect was observed on several contiguous temperature sensors within

the bubble area, they concluded that a micro-layer was deposited on the surface during bubble growth. The times between two bubbles were shown to vary significantly depending on experimental conditions and even sometimes during the same experiment but did not exceed 6 ms. Thanks to a numerical model of the wall using the measured temperature distribution beneath the bubble, the temporal and spatial variations of heat flux were obtained. With this procedure, they demonstrated an approximately even distribution of the dissipated heat between micro-layer evaporation, micro-convection in the liquid phase and transient heat conduction within the wall. Similarly, the presence of up to 1.2 mm long micro-layer is also deduced from the observed temperature variations by Yabuki et al. [39] as sustained and homogeneous temperature drops are witnessed along this radius beneath the bubble during its growth. Indeed, a strong impact of bubble growth on the thermal response of the wall is demonstrated as wall temperatures almost as low as the saturation temperature are measured below the bubble. In a more general manner, the authors of this study evaluate the waiting times between two bubbles at approximately 60 ms. Very similar conclusions were drawn in the case of subcooled boiling [46].

Using the IR visualisations of the heated substrate described above, Golobic et al. captured quick variations of the temperature field during bubble growth [40], as they are represented on Fig. 7. In this case, the bubble nucleation induced a significant cooling of the wall on the entire wall area located within the bubble followed by a progressive temperature recovery. Nevertheless, the very steep temperature fluctuations represented here are presumably a consequence of the very small thermal capacity of the foil heater. Due to these steep variations, they stated that the temporal resolution of the measures (1 ms) was still too large to capture the wall temperature distribution associated to the first phase of the bubble growth. It was thus difficult to conclude on the presence of a micro-layer beneath the bubble.

In the similar experiments conducted by Wagner & Stephan [41], the existence of a high heat flux ring area is highlighted near the observed junction between the bubble liquid/vapor interface and the wall. This was interpreted as the consequence of the rapidly moving micro-region in this area. However, the alternative possiblity of the existence of a micro-layer is not discussed. On the contrary, the sustained cooling of the wall on a length of the order of one millimeter is interpreted by Duan et al.[43] as a consequence of the presence of a micro-layer below the bubble. In the same time, they observed waiting times varying from 50 to 200 ms on the same substrate depending on the applied heat flux and nucleation temperature. However, the measured bubble growth times were approximately equal to 15 ms in any cases. These observations were globally consistent with the previous study of Gerardi et al. [42], as similar bubble dynamics and characteristic micro-layer wall temperature responses were highlighted.

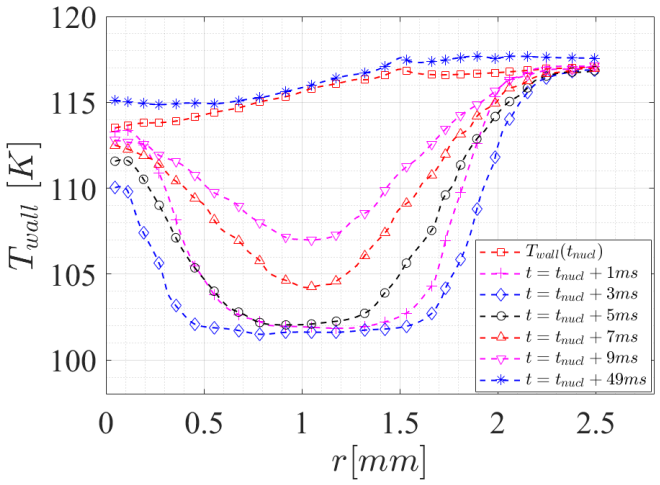

Figure 7: Measured wall temperature response during the bubble growth, adapted from Golobic et al. [40]

Thanks to their tri-camera setup, Jung et al. [45] closely correlated the strong temporal and spatial variations of the heat exchange intensity induced by the bubble growth and departure (represented on Fig. 8) to the liquid micro-layer identified with the optical interferometry apparatus. Additionally, the evaluation of the temperature field within the thickness of the substrate allowed to evaluate the area of influence of the bubble in the solid. In the radial direction, they highlighted a thermal influence radius approximately equal to the bubble radius, which is consistent with the thermal influence radius reported by Moghaddam et al. [38]. Along the thickness of the substrate, the thermal penetration length associated with the cycle of bubble nucleation was limited to around one millimeter. Such a limited area of influence of the bubble was confirmed by Giustini et al. [31] on the same experimental system for a higher applied heat flux. It is to be noted however than this observation has to be considered in light of the relatively low thermal diffusivity of the calcium fluoride wall ($\alpha_s \approx 2.10^{-6} m^2.s^{-1}$).

Finally, a significantly different wall temperature response was observed on both glass and sapphire heated substrates by Kangude & Srivastava [44].Indeed, in their setup, the area around the nucleation site remained at a constant overheat significantly higher than at its periphery. This result, contradictory with all the measurements and models reported above, has been explained in this study by the significant hydrophobicity of the surface inducing that a significant vapor volume remained attached to the nucleation site even after bubble departure. This was interpreted as preventing any micro-layer to form during bubble growth, thus inducing that the highest heat transfer were located close to the liquid/vapor interface.

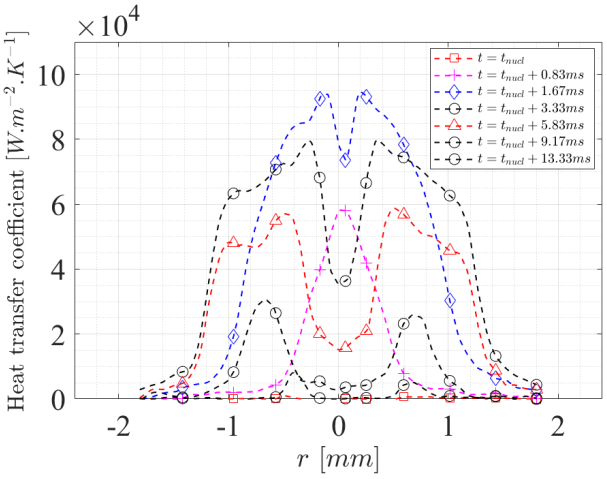

Figure 8: Local heat transfer coefficients during bubble growth deduced from the measured top surface temperature field, reproduced from Jung & Kim [45]

In addition, due to the significant difference in their thermal diffusivity, significantly lower temperature variations were observed for the sapphire than for the glass substrate for the same applied heat flux.

The main parameters and results of the experimental studies presented above are synthetized in Table 2. In this table, the geometry of the liquid/vapor interface close to the wall observed or inferred by the cited authors is indicated and the wall temperature response is quantified through the ratio $\frac{T_{nucl}-T_{wall}^{min}}{T_{nucl}-T_{sat}}$, in which T_{nucl} is the temperature at the nucleation site just before nucleation and T_{wall}^{min} is the lowest temperature measured on the solid beneath the bubble. Hence, a ratio equal to 0 indicates that no significant cooling within the wall is observed and, conversely, a ratio equal to 1 means that the solid wall is cooled down to the saturation temperature on at least one point.

From this summary, it appears that wide ranges of experimental configurations have been investigated, notably in terms of input heat flux, wall thickness and diffusivity. Hence, a set of data concerning wall thermal response and bubble dynamics is now available to the researcher for diverse entry parameters. Nevertheless, each experimental result is likely to be very specific to the corresponding experimental setup (for instance, to the input heat flux, nucleation superheat, fluid wettability and wall thickness). Considering this, the variation of output parameters between the different setups (wall thermal response and bubble dynamics in particular) is delicate to correlate to numerical parametric studies in which most of these parameters are held constant. To overcome this difficulty, it may be necessary to investigate single site nucleate boiling on substrates of varying thermal diffusivity in a unique experimental setup in which these parameters are held as constant as possible.

3. Thermal interaction within the wall on multiple nucleation sites

The previous sections focused on the interaction of a single bubble with the solid on which it grows. However, in most cases, a growing bubble is likely to be situated near multiple other bubbles. In this configuration, the local wall temperature variations induced by an active nucleation site may spread on a radius wide enough to affect the growth of close bubbles, as represented on Fig.9. Thus, it appears necessary to understand the practical effects of these interactions on multiple bubble growth as well as the distance at which they are significant, depending on the solid wall characteristics. To this end, the existing literature on the topic of thermal interactions within the heated wall between multiple nucleation sites is reviewed in this section. In a first part, the publications which investigate thermal interactions on heaters with well controlled artificial nucleation sites are presented. Then, studies on more conventional heaters having "natural" nucleation sites randomly disposed on the surface are discussed. Finally, published results on the wall material impact on the global boiling heat transfer coefficient are presented.

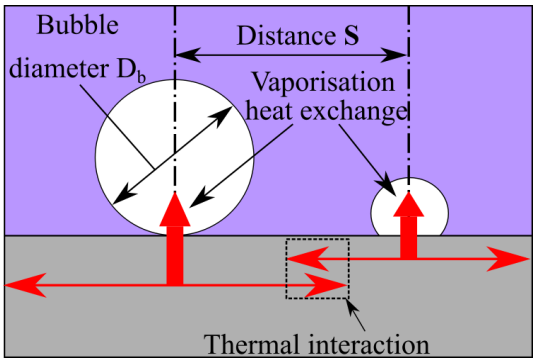

Figure 9: Schematic representation of the thermal interactions between two nucleations sites separated by a distance S

3.1. Interactions between regularly spaced artificial nucleation sites

To assess the influence of thermal interactions between adjacent sites as a function of the distance S between them, Zhang & Shoji investigated the boiling phenomena on several silicon substrate having two artificial nucleation sites with a different gap between them [47]. Local temperatures were measured with a radiation thermometer on the back side of the substrate. By calculating the correlation factor of the local temperature signal with the one of the nucleation site as a function of the distance S to the nucleation site, they were able to evaluate the intensity of thermal interaction within the wall. This interaction

Authors	α_s $[m^2/s]$	δ_{wall}	Fluid	φ $[W/cm^2]$	Observed bubble base	$\frac{T_{nucl}-T_{wall}^{min}}{T_{nucl}-T_{sat}}$	t_w $[ms]$	t_g $[ms]$
Myers et al. [37]	$7.7.10^{-7}$	500 μm	FC-72	$14-25$	micro-layer	0.1 (area averaged)	–	22
Wagner & Stephan [41]	4.10^{-6}	20 μm	FC-3284	$1.2-1.44$	micro-region	0.12	–	18
Golobic et al. [40]	$2.5.10^{-5}$	6 μm	water	$10-15$	-	0.9	40	9
Moghaddam et al. [38]	9.10^{-5} & $1.4.10^{-7}$	60 μm & 10 μm	FC-72	$0.5-3$	micro-layer	0.63	$0-6$	8
Duan et al. [43]	$7.8.10^{-6}$	250 μm	water	$2.9-3.6$	micro-layer	0.67	$50-200$	15
Gerardi et al. [42]	$7.8.10^{-6}$	400 μm	water	$0.2-100$	micro-layer	0.6	$50-100$	20
Kangude & Srivastava [44]	$3.4.10^{-7}$ $7.8.10^{-6}$	700 μm	water	$2.9-4.2$	-	0.6 0.1	0	250-300 50
Jung & Kim [45]	2.10^{-6}	1 cm	water	5.3	micro-layer	0.4	135	15
Yabuki & Nakabeppu [39]	9.10^{-5}	180 μm	water	–	micro-layer	1	60	18
Giustini et al. [31]	2.10^{-6}	1 cm	water	14.4	micro-layer	0.7	70	20

Table 2: Summary of the experimental configurations considered in the published studies and observed wall temperature response and bubble dynamics characteristics

was supposed to generally lower the nucleation frequency, due to the fact that the area around a nucleation site was relatively colder than its surroundings. In their particular setup, this interaction was shown to be present up to a dimensionless cavity spacing $S/\overline{D_b} = 2$, with $\overline{D_b}$ defined as the mean bubble diameter at departure. The same experimental setup was used to study a configuration with three nucleation sites placed in an inline or a triangular pattern [48, 49]. Similar conclusions were made in these publications, as the temperature correlation between a given point and the nucleation site was shown to quickly decreases with the distance to this point. The thermal interaction magnitude was evaluated as :

$$\Psi_t = \frac{\sum_i \rho_{c,i} + \sum_j \rho_{c,j}}{X_3 - X_1} \tag{1}$$

In this expression, ρ_{ci} and ρ_{cj} are the temperature correlation coefficients (defined as $\rho_{c,i} = \frac{cov(c,i)}{\sigma_c \times \sigma_i}$) between the cavity c and the other points i and j along a line connecting the two nucleation sites. The substraction $X_1 - X_3$ is the distance between the first and second cavity. As represented on Fig. 10, the influence of the geometrical configuration (inline or triangular) on the thermal interaction magnitude was relatively limited. Later, the analysis of experimental results obtained on this experimental configuration was conducted by Mosdorf & Shoji with the help of wavelet analysis [50]. The thermal interactions were shown to be negligible for $S/\overline{D_b} \geqslant 3$, which is consistent with the aforementioned results. Contrary to the conclusions of Zhang & Shoji, one of the conclusions of the study is that thermal interaction within the wall is beneficial to nucleation on both sites for $S/\overline{D_b} \leqslant 1.5$ and detrimental for $1.5 \leqslant S/\overline{D_b} \leqslant 3$. Finally, the same experimental setup was used to investigate boiling on thicker silicon substrates by Sato et al. [51]. In their case, the non-dimensionnal distance between sites was expressed as a function of the capillary length L_c. Thermal interactions were shown to be weaker than in the setup of Chatpun et al., which was explained by a different applied heat flux. In this case, they concluded that thermal interactions between sites were negligible for $S/L_c \geqslant 1.6$.

A different approach was used by Gjerkes & Golobic to evaluate sites interaction [52]. In their setup, a homogeneous heating is set at an intensity inducing the activation of a first nucleation site and a small diameter laser beam is used to activate a second site. Moving the laser beam then allows to vary the distance between the two sites while keeping the same substrate, in this case 25 μm thick copper or titanium foils. For both wall materials, the activity of the first nucleation site appears to decrease significantly when the distance with the second site is reduced, implying inhibitive interactions between sites. However, the specific effect of thermal conduction within the substrates is not discussed.

Furthermore, a numerical assessment of interactions between regularly spaced nucleation sites on a 380 μm thick silicon substrate was performed by Sanna et al. [53] and compared to numerical computations involving a thin titanium foil (similar to the one considered by Golobic et al. [40]). In the case of silicon, if nucleation was initially initiated at the same times for all nucleation sites, all the nucleation cycles remained synchronized during the entire simulation length. On the contrary, with the same initial condition, complete decoupling of the sites was achieved after a few nucleation cycles on the thin titanium foil. This was interpreted as an indication of stronger thermal interaction between sites within the silicon substrate. Finally, additional numerical results have been published by Zhang et al. [54] with the help of a lattice-boltzmann method applied to a two nucleation sites configuration. To assess thermal interactions between the two nucleation sites, they evaluated the temperature correlation coefficient ρ defined above. With this criterion, the interactions were shown to be strong up to $S/\overline{D_b} = 2$ (correlation coefficient $\rho > 0.5$) and became negligible for $S/\overline{D_b} = 2.9$ ($\rho = 0.004$). Within this range, the effect of thermal interactions was shown to lower the nucleation frequency. In addition, they showed

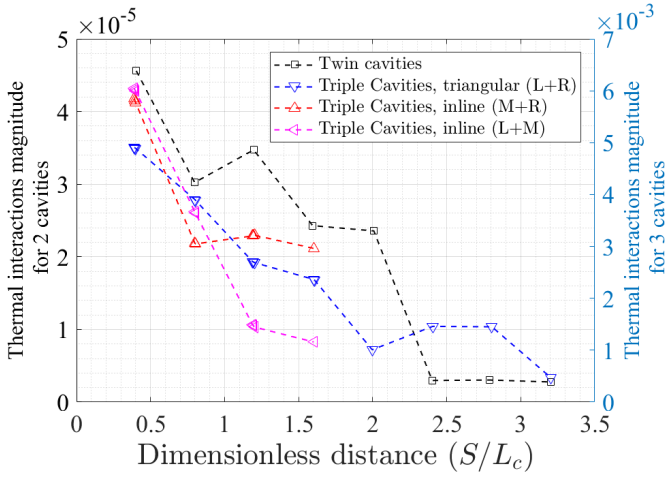

Figure 10: Measured intensity of the thermal interactions between adjacent sites, adapted from Chatpun et al. [48]

that as the wall superheat was increased, the intensity of thermal interactions can overcome the hydrodynamic interaction intensity.
In most of the studies presented above, the ratios $S/\overline{D_b}$ and S/L_c are used to specify the intensity of thermal interactions. However, as shown by the experimental study of Jiang et al., significantly different bubble dynamics can be observed for the same $S/\overline{D_b}$ value when the wall material is changed [55]. Indeed, the experimentally observed variations of bubble departure diameter and frequency with the ratio $S/\overline{D_b}$ was significantly different for 6 mm thick copper and stainless steel walls. Additionally, with the help of a numerical model, they demonstrated that thermal interactions were negligible within the copper wall, as temperature gradients remained very small regardless of the distance to the nucleation site. On the contrary, on a stainless steel surface, the temperature drops associated to two close cavities were non-negligible and overlapping, indicating significant thermal interactions between sites. Considering this, they recommend to consider a more comprehensive criterion taking into account wall properties to characterize thermal interactions between nucleation sites.

Indeed, to the best of the authors knowledge, the synthesis of the investigations, represented in table 3, shows that only a few wall configurations (defined here as the solid thermal diffusivity and thickness) have been investigated. Hence, despite the fact that the observed interactions range are comparable in these studies as they are only ranging between 1.6 and 3 bubble diameters, it is still difficult to provide a general interaction criterion at the moment. Thus, more experimental investigations on thermal interactions between controlled nucleation sites in various types of wall are needed to better understand the effect of thermal diffusivity on them.

3.2. Studies of conventional surfaces

Apart from the aforementionned publications focusing on thermal interactions between two or three artificial cavities, some researchers attempted to evaluate the effect and magnitude of thermal interactions within conventionnal walls, i.e. walls without artificial cavities but with natural ones. These studies are the subject of this section.

One of the first studies which address this question is the one conducted by Calka & Judd [56]. In their experimental investigation, 24 natural nucleation sites of a glass substrate were monitored. In a general manner, inhibiting interactions were observed for dimensionless nucleation sites spacing $S/\overline{D_b} < 1$ and promotive interactions were noticed for $1 < S/\overline{D_b} < 3$. It is to be noted that the overall thermal interaction range $0 < S/\overline{D_b} < 3$ is relatively consistent with the results obtained with artificial sites detailed in the section 3.1. However, in this case, the effects of thermal and hydrodynamic interactions are not separated. More recently, Kenning et al. [57] [58], with the help of thermosensitive liquid crystals deposited on a thin stainless steel heating foil, demonstrated that significant temperature gradients were induced by active natural nucleation sites on the back side of the heated substrate. Thermal interactions between sites were witnessed for dimensionless distances up to $S/\overline{D_b} \approx 1$. This relatively low interaction range was interpreted as a consequence of the thinness of the substrate (130 μm). Additionally, the sites characterized by a higher nucleation superheat, which induced the biggest bubbles, were shown to inhibit the nucleation of smaller bubbles around them. On the contrary, small nucleation sites did not have a significant impact on the bigger bubbles. These existing data were systematically processed with the help of non-orthogonal empirical functions (NEF) allowing to detect nucleation events by Von Hardenberg et al. [59] who pointed out similar interaction ranges. They however highlighted the fact that the observed value of non-dimensional interaction was highly dependant of the wall material and thickness.
Pool boiling on thin metallic foils has also been studied by Voglar et al. [60] by evaluating the statistical distribution of the local wall superheat on different wall materials. In this paper, they showed that much wider temperature fluctuations within the substrate were induced in the case of a stainless steel foil in comparison to a copper heater having the same dimensions.
More conventional aluminium and stainless steel substrates with thickness ranging from 6 to 11 mm were used by Chai et al. [61] who evaluated experimentally the thermal interaction by comparison of two nearby temperature measurements. In this setup, the interactions between the two temperatures measurements were shown to be stronger in the case of the 6 mm thick stainless steel substrate and lower for the more conductive 11 mm thick aluminium heater.

Authors	α_s $[m^2/s]$	δ_{wall}	Fluid	φ $[W/cm^2]$	Thermal interaction range	Thermal interaction effect
Zhang & Shoji [47]	9.10^{-5}	200 μm	water	$2.2-3.7$	$0 < S/\overline{D_b} < 2$	Decreased nucleation frequency
Chatpun et al. [48]	9.10^{-5}	200 μm	water	$3.4-5.6$	$0 < S/L_c < 3$	-
Mosdorf & Shoji [50]	9.10^{-5}	200 μm	water	2.65	$0 < S/\overline{D_b} < 1.67$	Inhibition of the nucleation
Sato et al. [51]	9.10^{-5}	500 μm	water	$2.5-3.7$	$0 < S/L_c < 1.6$	-
Gjerkes & Golobic [52]	$1.1.10^{-4}$ & 9.10^{-6}	25 μm	water	$0-3$	-	-
Zhang et al. [54]	-	-	water	–	$0 < S/\overline{D_b} < 2.9$	Decreased nucleation frequency
Jiang et al. [55]	$1.1.10^{-4}$ & 4.10^{-6}	6 mm	water	$3.3-7.3$	$0 < S/\overline{D_b} < 1.6$	Decreased departure diameter and nucleation frequency

Table 3: Heated wall characteristics, fluids considered by published studies and identified effects of thermal interaction on the bubble dynamics

To conclude this section, it appears that it is difficult to draw general conclusions from the few existing publications. Indeed, only a few configurations were studied and the random nature of natural nucleation sites distribution seemed to make difficult a quantitative analysis compared to studies inolving artificial nucleation sites where the dimensionless distance S/D_b was easier to control. It is however to be noted that the few observed orders of magnitude of interaction ranges appeared consistent with the results obtained on artificial sites.

3.3. Effect on heat transfer coefficient and critical heat flux

To conclude the review of multiple sites interactions, this section focuses on the more macroscopic approaches pursued by several authors who attempted to evaluate the effect of the heater material properties on the average heat transfer coefficient and critical heat flux.

In order to investigate the effect of wall material on the pool boiling heat transfer coefficient, Hosseini et al. performed boiling measurement on heaters made of copper, brass and aluminium [62]. To minimize the impact of different rugosities, all surfaces underwent the same polishing protocol. Overall, the brass and aluminium surfaces exhibited similar performances while an improvement of the heat transfer coefficient up to 20% was observed on the higher diffusivity copper substrate. A similar study, based on heaters made of copper, aluminium and stainless steel subjected to the same sanding process, has been proposed by Godinez et al. [63]. The highest heat transfer coefficients were measured with the highest thermal diffusivity copper heater and the lowest values were found for the lowest diffusivity substrate made of stainless steel. It is to be noted that heat transfer coefficient differences between the three materials were limited to approximately 10 to 20%. On the contrary, the measured values of critical heat fluxes (CHF) showed a different trend with copper having a significantly lower CHF than aluminium and stainless steel. This was explained as a consequence of the different surface wettabilities, since the boiling water was significantly more wetting on the aluminium than on the copper.
Instead of water, the pool boiling of nitrogen at cryogenic temperatures $(75-100\ K)$ was studied by Bombardieri et al. [64] on copper, aluminium and stainless steel. In terms of heat transfer coefficient, boiling on copper was again shown to be significantly more efficient than aluminium and stainless steel which were however more difficult to differentiate. On the other hand, significant differences on the critical heat fluxes between each of the materials were observed, ranging from 8.3 W/cm^2 for stainless steel to 20 W/cm^2 for copper and aluminium achieving an intermediate value 11.5 W/cm^2. Diamond and silicon carbide (SiC) substrates were compared as pool boiling substrates by Aus der Wiesche et al [65]. The two heaters induced a similar wettability of water and were polished to have similar rugosities. Heat transfer coefficients up to five times higher were measured on the diamond substrate compared to the SiC case. However, as detailed in a later publication [66], this specific observation might have been the consequence of additionnal nucleation beneath the heated substrate. Indeed, the use of additional sealing around the heater (preventing fluid flow beneath it) resulted in almost identical boiling curves for the two materials. In fact, the silicon carbide even induced a slightly higher heat transfer coefficient than the diamond one despite its much lower thermal diffusivity. This counterintuitive difference was explained as the consequence of a higher nucleation site density on the silicon carbide substrate.

In the case of thin metallic foils, the comparative study led by Voglar et al. [60] cited in section 3.2 gave some insight on the wall properties effect on the boiling heat transfer coefficient. Indeed, the copper foil induced an approximately doubled boiling heat transfer coefficient compared to the steel surface. However, it is to be noted that this observed difference may also be a consequence of the addition of nanostructurations on the copper foil while the stainless steel surface did not receive any surface treatment.

A different gemetrical configuration in which a cylindrical heater was used to induce nucleate boiling has also been investigated by other researchers. Jabardo et al. compared the boiling of refrigerants R-134a and R-123 on stainless steel, brass and copper rods [67]. Overall, the boiling heat transfer coefficient and critical heat flux were shown to

increase with the heater thermal diffusivity. In terms of heat transfer coefficient, the difference between materials was particularly visible at high heat fluxes, i.e. close to critical heat flux. In addition, rougher surfaces tended to induce higher differences between the materials. For the same geometry of heaters, to provide guidance in the choice of material used in nuclear reactor coolers, Seo et al. compared zirconium and SiC heaters during pool boiling of distilled water [68]. As the SiC heater was characterized by a much higher thermal diffusivity, the heat transfer coefficient was shown to be approximately doubled compared to the zirconium cylinder. Furthermore, a 63% improvement of the critical heat flux was observed with the silicon carbide wall.

Finally, on the particular topic of CHF associated to pool boiling of water, a significant finding was highlighted by Raghupathi & Kandlikar as they experimentally compared the CHF associated to pool boiling of water on heaters made of 6 different materials [69]. Indeed, they showed that the ratio between the measured CHF and the one predicted by a preexisting CHF predicting tool almost linearly increases with the parameter $\sqrt{\rho Cp}$, with ρ and Cp being the density and heat capacity of the heater. The addition of a corrective term $\sqrt{\rho Cp}_{heater}/\sqrt{\rho Cp}_{copper}$ to this CHF model then allowed to obtain valid predictions of CHF for 7 different materials.
A synthesis of these experimental configurations and related observations is detailed in Table 4. For the sake of concision, only 3 of the 6 materials considered by Raghupathi & Kandlikar are reported in this table.

However, the numerical investigation of wall thermal properties influence on heat transfer coefficient does not appear to be the object of many studies. First, a numerical study based on previously mentioned Lattice Boltzmann method has been conducted by Gong et al. [70], allowing to discuss the influence of the wall thermal properties on the computed boiling curve. In a general manner, they state that the influence of the wall thermal conductivity on the boiling curve is very limited. Additionally, a CFD modelling of pool boiling on various surfaces having randomly dispersed nucleation sites and taking into account thermal coupling with the heated wall has been proposed by Petrovic & Stevanovic [71]. Thanks to some simplifications of the two phase flow modelling and associated heat transfer, they showed the possibility to realize 3D simulations of pool boiling over the entire heater area. The numerical results showed in particular that, for the same dissipated heat flux and nucleation site density, the mean overheat of the solid surface in contact with the fluid could be doubled when its material was changed from copper to stainless steel.

To synthesize this section of the review, two global conclusions can be drawn. First, in terms of heat transfer coefficients, most studies tend to agree on the fact that a heater having a high thermal diffusivity, typically made of copper, tends to induce higher heat transfer coefficients than lower diffusivity heaters, typically made of stainless steel. However, the actual significance of this variation seems to vary greatly among the authors cited in this review. At this stage, these discrepancies may simply be explained by other parameters such as the fluid used as well as surface roughness and wettability, which can vary significantly between the reported experiments. Concerning the variations of critical heat flux with the heater material, the thermal diffusivity variations do not seem to explain the observed variations. On the contrary, the parameter $\sqrt{\rho Cp}$ recently proposed by Raghupathi & Kandlikar [69] might to be a promising tool for the CHF evaluation.

4. Synthesis and conclusions

As discussed in the introduction, the review presented in this paper intentionally overlooked several phenomenon fundamental to nucleate boiling which have already been broadly discussed in the published literature, in particular the effect of fluid wettability and solid wall geometry on nucleate boiling. However, this relatively narrow framework enabled to draw some general conclusions on the specific influence of the wall material on single bubble dynamics as well as thermal interactions between bubbles through the wall.

First, the quantitative influence of the wall thermal properties on single bubble dynamics has been evaluated by several authors thanks to numerical simulations coupling liquid/vapor hydrodynamics with conduction within the wall. In these simulations, a significant inhibition of bubble growth was associated with a reduction of the wall thermal diffusivity when micro-layer deposition was considered at the base of the bubble. On the other hand, contradictory results emerged from models that did not consider any micro-layer beneath the bubble. However, to the best of the authors knowledge, such conclusions are only limited to a few numerical studies meaning that additionnal numerical investigations may be necessary to confirm these observations.
Simultaneously, thanks to specially developed experimental procedures, several papers demonstrated the possibility to obtain experimental data of heat transfer and temperature fields within the heated wall beneath a growing bubble. This allowed to quantify heat transfer within the wall as well as the bubble base geometry on a few particular configurations. However, these experiments are by nature specific to a given heated substrate. It is hence difficult to infer the wall thermal properties influence on the nucleation process from these results. For the same reason, comparison of these experimental data with the aforementionned numerical results seems to be delicate at the moment.
Concerning the broader topic of multi-sites boiling, several

Authors	Wall material	Fluid	Contact angle	Surface roughness [μm]	Highest observed effect on HTC/CHF
Hosseini et al. [62]	brass aluminium copper	R113	- - -	Ra = 1.404 Ra = 0.901 Ra = 1.285	ref - +20% on HTC
Godinez et al. [63]	stainless steel aluminium copper	water	49 12 65	Ra = 0.1 Ra = 0.8 Ra = 0.2	ref +10% on HTC/+35% on CHF +20% on HTC/−25% on CHF
Bombardieri et al. [64]	stainless steel aluminium copper	Liquid nitrogen	close to 0 close to 0 close to 0	Ra = 0.117 Ra = 0.141 Ra = 0.076	ref similar HTC/+40% on CHF +200% on HTC / +140% on CHF
Aus der wiesche et al [65]	Silicon carbide diamond	water	$40-45^o$ $40-45^o$	Ra = 0.15 Ra = 0.22	HTC on diamond flawed by nucleation below the substrate
Kapitz et al [66]	Silicon carbide diamond	water	42.9^o 39.1^o	Ra = 0.15 Ra = 0.22	ref −30% on HTC
Voglar et al. [60]	stainless steel titanium copper	water	88^o 93^o 0^o	Ra = 0.07 Ra = 0.33 Ra = 0.30	ref +33% on HTC +100% on HTC (nanostructured surface)
Jabardo et al. [67]	stainless steel brass copper	R134a and R123	- - -	Ra = 0.03-3 Ra = 0.08-3.5 Ra = 0.07-10.5	ref +150% on HTC +400% on HTC
Seo et al. [67]	zirconium silicon carbide	water	85^o 93^o	Ra = 0.088 Ra = 0.107	ref +150% on HTC +400% on HTC
Raghupathi & Kandlikar [69]	carbon steel silver copper	water	26 21 40	Ra = 1.21 Ra = 1.4 Ra = 0.93	ref −25% on CHF −18% on CHF

Table 4: Heated wall characteristics, fluids considered by published studies and identified effects of the wall material on the overall heat transfer

approaches were developed in the past decades to evaluate the interactions between nucleation sites through solid conduction within the wall. A common considered parameter was the distance between sites divided by the mean bubble diameter at departure. Although some interaction ranges based on this parameter were proposed, several authors pointed out the fact that these criteria were only valid for a specific wall material and thickness. Hence, a more general criterion of interaction range taking into account the solid wall characteristics is yet to be determined. Finally, on a macroscopic point of view, more conductive boiling substrates were in general shown to induce higher heat transfer coefficients and critical heat fluxes. However, this conclusion remains mostly empirical at the present day. Hence, the comprehension of the complex influence of the wall properties on the overall heat transfer remains a challenging task.

To conclude, this brief review permitted to show that, thanks to recent advances in both numerical and experimental, significant progress has been made in the understanding of the thermal coupling between nucleating bubbles and the solid wall on which they grow. Nevertheless, further research may still be necessary to improve this current understanding. In particular, to the best of the authors' knowledge, new experimental investigations of different wall materials associated to a comparison to numerical results remain to be done. Indeed, many other crucial parameters such as surface roughness, fluid wettability and nucleation superheat are different from one experimental setup to the others. At longer term, a more detailed physical understanding of this particular topic may be necessary to establish general criteria as well as predictive tools to design a boiling surface as a function of its constitutive material. For instance, such tools may be valuable to allow a decrease in the weight of cooling systems based on nucleate boiling heat transfer, by the use of lightweight materials such as polymer or by thinning solid walls.

Conflict of interest

None declared.

References

[1] D. Gorenflo, S. Kotthoff, Review on pool boiling heat transfer of carbon dioxide, International Journal of Refrigeration 28 (8) (2005) 1169–1185.

[2] K. Leong, J. Ho, K. Wong, A critical review of pool and flow boiling heat transfer of dielectric fluids on enhanced surfaces, Applied Thermal Engineering 112 (2017) 999–1019.

[3] V. K. Dhir, G. R. Warrier, E. Aktinol, Numerical simulation of pool boiling: a review, Journal of Heat Transfer 135 (6) (2013).

[4] S. Noie, Heat transfer characteristics of a two-phase closed thermosyphon, Applied Thermal Engineering 25 (4) (2005) 495–506.

[5] B. Fadhl, L. C. Wrobel, H. Jouhara, Numerical modelling of the temperature distribution in a two-phase closed thermosyphon, Applied Thermal Engineering 60 (1-2) (2013) 122–131.

[6] H. Shabgard, B. Xiao, A. Faghri, R. Gupta, W. Weissman, Thermal characteristics of a closed thermosyphon under various filling conditions, International Journal of Heat and Mass Transfer 70 (2014) 91–102.

[7] R. L. Mohanty, M. K. Das, A critical review on bubble dynamics parameters influencing boiling heat transfer, Renewable and Sustainable Energy Reviews 78 (2017) 466–494.

[8] I. Malavasi, E. Teodori, A. S. Moita, A. L. Moreira, M. Marengo, Wettability effect on pool boiling: a review, Encyclopedia of Two-Phase Heat Transfer and Flow III (2018) 1–61.

[9] J. Kim, Review of nucleate pool boiling bubble heat transfer mechanisms, International Journal of Multiphase Flow 35 (12) (2009) 1067–1076.

[10] G. Liang, I. Mudawar, Review of pool boiling enhancement by surface modification, International Journal of Heat and Mass Transfer 128 (2019) 892–933. doi:10.1016/j.ijheatmasstransfer.2018.09.026.

[11] A. Shahriari, P. Birbarah, J. Oh, N. Miljkovic, V. Bahadur, Electric field–based control and enhancement of boiling and condensation, Nanoscale and Microscale Thermophysical Engineering 21 (2) (2017) 102–121.

[12] I. Pioro, W. Rohsenow, S. Doerffer, Nucleate pool-boiling heat transfer. i: review of parametric effects of boiling surface, International Journal of Heat and Mass Transfer 47 (23) (2004) 5033–5044.

[13] A. Mehralizadeh, S. R. Shabanian, G. Bakeri, Effect of modified surfaces on bubble dynamics and pool boiling heat transfer enhancement: A review, Thermal Science and Engineering Progress (2019) 100451.

[14] M. S. El-Genk, Z. Guo, Liquid microlayer evaporation during nucleate boiling on the surface of a flat composite wall, International Journal of Heat and Mass Transfer 37 (11) (1994) 1641–1655. doi:10.1016/0017-9310(94)90179-1.

[15] R. Mei, W. Chen, J. F. Klausner, Vapor bubble growth in heterogeneous boiling—I. Formulation, International Journal of Heat and Mass Transfer 38 (5) (1995) 909–919. doi:10.1016/0017-9310(94)00195-2.

[16] R. Mei, W. Chen, J. F. Klausner, Vapor bubble growth in heterogeneous boiling—II. Growth rate and thermal fields, International Journal of Heat and Mass Transfer 38 (5) (1995) 921–934. doi:10.1016/0017-9310(94)00196-3.

[17] M. Mann, K. Stephan, P. Stephan, Influence of heat conduction in the wall on nucleate boiling heat transfer, Int. J. Heat Mass Transfer (2000) 11.

[18] T. Fuchs, J. Kern, P. Stephan, A Transient Nucleate Boiling Model Including Microscale Effects and Wall Heat Transfer, Journal of Heat Transfer 128 (12) (2006) 1257–1265. doi:10.1115/1.2349502.

[19] P. Stephan, T. Fuchs, Local heat flow and temperature fluctuations in wall and fluid in nucleate boiling systems, Heat and Mass Transfer 45 (7) (2009) 919–928. doi:10.1007/s00231-007-0320-1.

[20] C. Kunkelmann, P. Stephan, Numerical simulation of the transient heat transfer during nucleate boiling of refrigerant hfe-7100, International Journal of Refrigeration 33 (7) (2010) 1221–1228.

[21] E. Aktinol, V. K. Dhir, Numerical Simulation of Nucleate Boiling Phenomenon Coupled with Thermal Response of the Solid, Microgravity Science and Technology 24 (4) (2012) 255–265. doi:10.1007/s12217-012-9308-7.

[22] Y. Y. Jiang, H. Osada, M. Inagaki, N. Horinouchi, Dynamic modeling on bubble growth, detachment and heat transfer for hybrid-scheme computations of nucleate boiling, International Journal of Heat and Mass Transfer 56 (1-2) (2013) 640–652. doi:10.1016/j.ijheatmasstransfer.2012.09.006.

[23] L. Zhang, Z.-D. Li, K. Li, H.-X. Li, J.-F. Zhao, Influence of heater thermal capacity on bubble dynamics and heat transfer in nucleate pool boiling, Applied Thermal Engineering 88 (2015) 118–126. doi:10.1016/j.applthermaleng.2014.11.080.

[24] Z.-D. Li, L. Zhang, J.-F. Zhao, H.-X. Li, K. Li, K. Wu, Numerical simulation of bubble dynamics and heat transfer with transient thermal response of solid wall during pool boiling of FC-72, International Journal of Heat and Mass Transfer 84 (2015) 409–418. doi:10.1016/j.ijheatmasstransfer.2014.12.061.

[25] P. A. Raghupathi, S. G. Kandlikar, Bubble growth and departure trajectory under asymmetric temperature conditions, International Journal of Heat and Mass Transfer 95 (2016) 824–832. doi:10.1016/j.ijheatmasstransfer.2015.12.058.

[26] S. Gong, P. Cheng, X. Quan, Two-dimensional mesoscale simulations of saturated pool boiling from rough surfaces. part i: Bubble nucleation in a single cavity at low superheats, International Journal of Heat and Mass Transfer 100 (2016) 927–937.

[27] G. Huber, S. Tanguy, M. Sagan, C. Colin, Direct numerical simulation of nucleate pool boiling at large microscopic contact angle and moderate Jakob number, International Journal of Heat and Mass Transfer 113 (2017) 662–682. doi:10.1016/j.ijheatmasstransfer.2017.05.083.

[28] G. Giustini, S. Walker, Y. Sato, B. Niceno, Computational fluid dynamics analysis of the transient cooling of the boiling surface at bubble departure, Journal of Heat Transfer 139 (9) (2017).

[29] Z. Chen, F. Wu, Y. Utaka, Numerical simulation of thermal property effect of heat transfer plate on bubble growth with microlayer evaporation during nucleate pool boiling, International Journal of Heat and Mass Transfer 118 (2018) 989–996. doi:10.1016/j.ijheatmasstransfer.2017.11.083.

[30] Z. Wang, M. Z. Podowski, Analytical modeling of the effect of heater geometry on boiling heat transfer, Nuclear Engineering and Design 344 (2019) 122–130. doi:10.1016/j.nucengdes.2018.12.020.

[31] G. Giustini, I. Kim, H. Kim, Comparison between modelled and measured heat transfer rates during the departure of a steam bubble from a solid surface, International Journal of Heat and Mass Transfer 148 (2020) 119092. doi:10.1016/j.ijheatmasstransfer.2019.119092.

[32] C. R. Kharangate, I. Mudawar, Review of computational studies on boiling and condensation, International Journal of Heat and Mass Transfer 108 (2017) 1164–1196.

[33] P. Stephan, C. Busse, Analysis of the heat transfer coefficient of grooved heat pipe evaporator walls, International Journal of heat and mass transfer 35 (2) (1992) 383–391.

[34] S. Jung, H. Kim, Hydrodynamic formation of a microlayer underneath a boiling bubble, International Journal of Heat and Mass Transfer 120 (2018) 1229–1240.

[35] S. Fischer, T. Gambaryan-Roisman, P. Stephan, On the development of a thin evaporating liquid film at a receding liquid/vapour-interface, International Journal of Heat and Mass Transfer 88 (2015) 346–356.

[36] K. Schweikert, A. Sielaff, P. Stephan, On the transition between contact line evaporation and microlayer evaporation during the dewetting of a superheated wall, International Journal of Thermal Sciences 145 (2019) 106025.

[37] J. G. Myers, V. K. Yerramilli, S. W. Hussey, G. F. Yee, J. Kim, Time and space resolved wall temperature and heat flux measurements during nucleate boiling with constant heat flux boundary conditions, International Journal of Heat and Mass Transfer 48 (12) (2005) 2429–2442. doi:10.1016/j.ijheatmasstransfer.2004.12.050.

[38] S. Moghaddam, K. Kiger, Physical mechanisms of heat transfer during single bubble nucleate boiling of FC-72 under saturation conditions-I. Experimental investigation, International Journal of Heat and Mass Transfer 52 (5-6) (2009) 1284–1294. doi:10.1016/j.ijheatmasstransfer.2008.08.018.

[39] T. Yabuki, O. Nakabeppu, Heat transfer mechanisms in isolated bubble boiling of water observed with MEMS sensor, International Journal of Heat and Mass Transfer 76 (2014) 286–297. doi:10.1016/j.ijheatmasstransfer.2014.04.012.

[40] I. Golobic, J. Petkovsek, M. Baselj, A. Papez, D. Kenning, Experimental determination of transient wall temperature distributions close to growing vapor bubbles, Heat and mass transfer 45 (7) (2009) 857–866.

[41] E. Wagner, P. Stephan, High-Resolution Measurements at Nucleate Boiling of Pure FC-84 and FC-3284 and Its Binary

Mixtures, Journal of Heat Transfer 131 (12) (2009) 121008. doi:10.1115/1.3220143.
[42] C. Gerardi, J. Buongiorno, L.-w. Hu, T. McKrell, Study of bubble growth in water pool boiling through synchronized, infrared thermometry and high-speed video, International Journal of Heat and Mass Transfer 53 (19-20) (2010) 4185–4192.
[43] X. Duan, B. Phillips, T. McKrell, J. Buongiorno, Synchronized High-Speed Video, Infrared Thermometry, and Particle Image Velocimetry Data for Validation of Interface-Tracking Simulations of Nucleate Boiling Phenomena, Experimental Heat Transfer 26 (2-3) (2013) 169–197. doi:10.1080/08916152.2012.736837.
[44] P. Kangude, A. Srivastava, Understanding the growth mechanism of single vapor bubble on a hydrophobic surface: Experiments under nucleate pool boiling regime, International Journal of Heat and Mass Transfer 154 (2020) 119775.
[45] S. Jung, H. Kim, An experimental method to simultaneously measure the dynamics and heat transfer associated with a single bubble during nucleate boiling on a horizontal surface, International Journal of Heat and Mass Transfer 73 (2014) 365–375. doi:10.1016/j.ijheatmasstransfer.2014.02.014.
[46] T. Yabuki, O. Nakabeppu, Microscale wall heat transfer and bubble growth in single bubble subcooled boiling of water, International Journal of Heat and Mass Transfer 100 (2016) 851–860. doi:10.1016/j.ijheatmasstransfer.2016.04.112.
[47] L. Zhang, M. Shoji, Nucleation site interaction in pool boiling on the artificial surface, International Journal of Heat and Mass Transfer 46 (3) (2003) 513–522. doi:10.1016/S0017-9310(02)00291-0.
[48] S. Chatpun, M. Watanabe, M. Shoji, Nucleation site interaction in pool nucleate boiling on a heated surface with triple artificial cavities, International journal of heat and mass transfer 47 (14-16) (2004) 3583–3587.
[49] S. Chatpun, M. Watanabe, M. Shoji, Experimental study on characteristics of nucleate pool boiling by the effects of cavity arrangement, Experimental Thermal and Fluid Science 29 (1) (2004) 33–40. doi:10.1016/j.expthermflusci.2004.01.007.
[50] R. Mosdorf, M. Shoji, Temperature fluctuation at twin cavity in nucleate boiling—wavelet analysis and modelling, International Journal of Heat and Mass Transfer 49 (17-18) (2006) 3156–3166. doi:10.1016/j.ijheatmasstransfer.2006.02.010.
[51] T. Sato, Y. Koizumi, H. Ohtake, Experimental study on fundamental phenomena of boiling using heat transfer surfaces with well-defined cavities created by mems (effect of spacing between cavities), Journal of heat transfer 130 (8) (2008).
[52] H. Gjerke, Measurement of certain parameters in¯uencing activity of nucleation sites in pool boiling, Experimental Thermal and Fluid Science (2002) 7.
[53] A. Sanna, C. Hutter, D. Kenning, T. Karayiannis, K. Sefiane, R. Nelson, Numerical investigation of nucleate boiling heat transfer on thin substrates, International Journal of Heat and Mass Transfer 76 (2014) 45–64.
[54] L. Zhang, T. Wang, S. Kim, Y. Jiang, The effects of wall superheat and surface wettability on nucleation site interactions during boiling, International Journal of Heat and Mass Transfer 146 (2020) 118820. doi:10.1016/j.ijheatmasstransfer.2019.118820.
[55] Y. Y. Jiang, H. Osada, M. Inagaki, N. Horinouchi, Wall Thermal Conductivity Effects on Nucleation Site Interaction During Boiling: An Experimental Study, in: 2010 14th International Heat Transfer Conference, Volume 1, ASMEDC, Washington, DC, USA, 2010, pp. 637–646. doi:10.1115/IHTC14-23140.
[56] A. Calka, R. L. Judd, Some aspects of the interaction among nucleation sites during saturated nucleate boiling, International journal of heat and mass transfer 28 (12) (1985) 2331–2342.
[57] D. Kenning, Wall temperature patterns in nucleate boiling, International journal of heat and mass transfer 35 (1) (1992) 73–86.
[58] D. Kenning, Y. Yan, Pool boiling heat transfer on a thin plate: features revealed by liquid crystal thermography, International Journal of Heat and Mass Transfer 39 (15) (1996) 3117–3137. doi:10.1016/0017-9310(96)00006-3.
[59] J. von Hardenberg, D. B. Kenning, H. Xing, L. Smith, Identification of nucleation site interactions, International Journal of Heat and Fluid Flow 25 (2) (2004) 298–304. doi:10.1016/j.ijheatfluidflow.2003.11.015.
[60] J. Voglar, M. Zupančič, A. Peperko, P. Birbarah, N. Miljkovic, I. Golobič, Analysis of heater-wall temperature distributions during the saturated pool boiling of water, Experimental Thermal and Fluid Science 102 (2019) 205–214. doi:10.1016/j.expthermflusci.2018.11.012.
[61] L. Chai, X. Peng, B. Wang, Nucleation site interaction during boiling, International journal of heat and mass transfer 43 (23) (2000) 4249–4258.
[62] H. Reza, G. Amir, N. Mahdi, Concerning the effect of surface material on nucleate boiling heat transfer of r-113, Journal of Electronics Cooling and Thermal Control 2011 (2011).
[63] J. C. Godinez, H. Cho, D. Fadda, J. Lee, S. J. Park, S. M. You, Effects of materials and microstructures on pool boiling of saturated water from metallic surfaces, International Journal of Thermal Sciences 165 (2021) 106929.
[64] C. Bombardieri, C. Manfletti, Influence of wall material on nucleate pool boiling of liquid nitrogen, International Journal of Heat and Mass Transfer 94 (2016) 1–8. doi:10.1016/j.ijheatmasstransfer.2015.10.049.
[65] S. aus der Wiesche, U. Bardas, S. Uhkötter, Boiling heat transfer on large diamond and SiC heaters: The influence of thermal wall properties, International Journal of Heat and Mass Transfer 54 (9-10) (2011) 1886–1895. doi:10.1016/j.ijheatmasstransfer.2010.12.032.
[66] M. Kapitz, A. Becker, S. a. d. Wiesche, Influence of Thermophysical Wall Properties During Pool Boiling on Large Diamond and SiC Heaters, Heat Transfer Engineering 35 (5) (2014) 472–481. doi:10.1080/01457632.2013.833046.
[67] J. M. S. Jabardo, G. Ribatski, E. Stelute, Roughness and surface material effects on nucleate boiling heat transfer from cylindrical surfaces to refrigerants r-134a and r-123, Experimental Thermal and Fluid Science 33 (4) (2009) 579–590.
[68] G. H. Seo, G. Jeun, S. J. Kim, Pool boiling heat transfer characteristics of zircaloy and SiC claddings in deionized water at low pressure, Experimental Thermal and Fluid Science 64 (2015) 42–53. doi:10.1016/j.expthermflusci.2015.01.017.
[69] P. A. Raghupathi, S. G. Kandlikar, Effect of thermophysical properties of the heater substrate on critical heat flux in pool boiling, Journal of Heat Transfer 139 (11) (2017).
[70] S. Gong, P. Cheng, Direct numerical simulations of pool boiling curves including heater's thermal responses and the effect of vapor phase's thermal conductivity, International Communications in Heat and Mass Transfer 87 (2017) 61–71. doi:10.1016/j.icheatmasstransfer.2017.06.023.
[71] M. M. Petrovic, V. D. Stevanovic, Coupled two-fluid flow and wall heat conduction modeling of nucleate pool boiling, Numerical Heat Transfer, Part A: Applications (2021) 1–29.